Published in final edited form as:
Invest Ophthalmol Vis Sci. 2009 February ; 50(2): 820–825. doi:10.1167/iovs.08-2343.

Three-Dimensional Mapping of Chorioretinal Vascular Oxygen Tension in the Rat

Mahnaz Shahidi, **Justin Wanek**, **Norman P. Blair**, and **Marek Mori**
Department of Ophthalmology and Visual Sciences, University of Illinois at Chicago, Chicago, Illinois

Abstract

Purpose—An optical section phosphorescence lifetime imaging system was developed for three-dimensional mapping of oxygen tension (PO_2) in chorioretinal vasculatures.

Methods—A laser line was projected at an oblique angle and scanned on the retina after intravenous injection of an oxygen-sensitive molecular probe to generate phosphorescence optical section images. An automated software algorithm segmented and combined images from spatially adjacent locations to construct depth-displaced en face retinal images. Intravascular PO_2 was measured by determining the phosphorescence lifetime. Three-dimensional chorioretinal PO_2 maps were generated in rat eyes under varying fractions of inspired oxygen.

Results—Under an air-breathing condition, mean PO_2 in the choroid, retinal arteries, capillaries, and veins were 58 ± 2 mm Hg, 47 ± 2 mm Hg, 44 ± 2 mm Hg, and 35 ± 2 mm Hg, respectively. The mean arteriovenous PO_2 difference was 12 ± 2 mm Hg. With a lower fraction of inspired oxygen, chorioretinal vascular PO_2 and mean arteriovenous PO_2 differences decreased compared with measurements under an air-breathing condition. Retinal venous PO_2 was statistically lower than PO_2 measured in the retinal artery, capillaries, and choroid ($P < 0.004$).

Conclusions—Three-dimensional mapping of chorioretinal oxygen tension allowed quantitative PO_2 measurements in large retinal blood vessels and in retinal capillaries. This method has the potential to facilitate better understanding of retinal oxygenation in health and disease.

Abnormalities in retinal oxygen delivery and consumption are thought to play significant roles in common retinal diseases, among them diabetic retinopathy and vascular occlusion. Thus far, however, knowledge of fundamental mechanisms that implicate oxygen in the development of retinal abnormalities remains deficient and sparse. Noninvasive technologies that allow the assessment of oxygen tension (PO_2) in chorioretinal vasculatures and retinal tissue are greatly needed to broaden knowledge of disease pathophysiology and thereby advance diagnostic and therapeutic procedures.

Several techniques have been developed to assess PO_2 in the retinal tissue and vasculature. Retinal tissue PO_2 has been directly measured with high-depth resolution using oxygen-sensitive microelectrodes,[1–12] but measurements are limited to one-dimensional linear profiles through retinal depth. Although in principle multiple line profiles may be derived, in practice this process is time consuming and may disturb the retinal microenvironment. Magnetic resonance imaging (MRI) has been used to study changes in preretinal oxygenation,[13–18] but it does not provide an absolute measurement of tissue PO_2, and it has lower resolution than optical techniques. Multi-wavelength reflectance spectrophotometry has provided

Corresponding author: Mahnaz Shahidi, Department of Ophthalmology and Visual Sciences, University of Illinois at Chicago, 1855 West Taylor Street, Chicago, IL 60612; mahnshah@uic.edu.

Disclosure: **M. Shahidi**, None; **J. Wanek**, None; **N.P. Blair**, None; **M. Mori**, None

measurements of blood oxygen saturation in retinal vasculatures. [19–27] However, the relationship between PO_2 and oxygen saturation of hemoglobin is determined by the oxygen-hemoglobin dissociation curve, which may be altered because of various metabolic conditions. Additionally, measurements of oxygen saturation are limited to large retinal blood vessels and technically are not achievable in retinal capillaries. Measurements of retinal oxygen tension and consumption[28] and retinal vascular PO_2[16,29–36] have been reported based on fluorescence and phosphorescence quenching of molecular probes, respectively. However, these imaging methods lack adequate depth resolution and only detect fluorescence or phosphorescence from the entire retinal thickness and choroid. Specifically, retinal capillary PO_2 measurements are not accurate with these methods because measurements are higher than retinal arterial measurements,[35] a result that is not physiologically plausible. The contribution of phosphorescence from the choroid is the most likely explanation for these measurement errors.

We have previously developed a novel system for optical section phosphorescence imaging. The system has been used to generate two-dimensional (2D) PO_2 maps through retinal depth and to quantitatively measure PO_2 separately in the choroidal and retinal vasculatures.[37–39] In the present study, we report further development of our system for three-dimensional (3D) mapping of PO_2 in the chorioretinal vasculatures. Our system generates en face PO_2 maps at different retinal depths, allowing quantitative PO_2 measurements in the choroid, retinal arteries, capillaries, and veins, as well as evaluation of vascular PO_2 variations in horizontal retinal planes. En face chorioretinal vascular PO_2 maps are useful for identifying potentially vulnerable retinal areas, in terms of oxygenation, in diseases such as diabetic retinopathy and macular degeneration. Furthermore, mapping of retinal vascular PO_2 improves understanding of oxygen gradients along retinal vasculatures.

Methods

Animals

Male Long Evans pigmented rats (weight range, 450–650 g; $n = 10$) were used for this study. The animals were treated in compliance with the ARVO Statement for the Use of Animals in Ophthalmic and Vision Research and were anesthetized with ketamine (85 mg/kg intraperitoneally) and xylazine (3.5 mg/kg intraperitoneally). Anesthesia was maintained by intraperitoneal infusion of ketamine and xylazine at the rate of 0.5 mg/kg/min and 0.02 mg/kg/min, respectively. The femoral artery was cannulated, and a catheter was attached for drawing arterial blood and monitoring each animal's physiological condition. During imaging, the blood pressure of the animals was monitored through a pressure transducer linked to a femoral artery catheter and a data acquisition system (Biopac Systems, Goleta, CA). Body temperature was maintained through a copper tubing water heater and was monitored with a rectal thermometer. The fraction of inspired oxygen was varied in nine rats through a high-flow face mask system. Gas mixtures containing 10% oxygen (hypoxia) or 21% oxygen (room air, normoxia) were administered to rats for 5 minutes before and during imaging. Concurrent with imaging, arterial blood (200 μL) was drawn through the catheter without air exposure, and systemic arterial PO_2 was measured with use of a blood gas analyzer (Radiometer, Westlake, OH).

Pupils were dilated with 2.5% phenylephrine and 1% tropicamide. An oxygen-sensitive molecular probe, Pd-porphine (Frontier Scientific, Logan, UT), was dissolved (12 mg/mL) in bovine serum albumin solution (60 mg/mL) and physiological saline buffered to pH 7 and was injected intravenously (20 mg/kg). Before imaging, 1% hydroxypropyl methylcellulose was applied to the cornea, and a glass coverslip was placed on the cornea to eliminate its refractive power and to prevent corneal dehydration. The rat was placed in front of the imaging instrument. The laser power was adjusted to 100 mW, which is safe for viewing according to

the American National Standard Institute for Safety Standards.[40] Imaging was performed at areas within 2 disc diameters (600 μm) from the edge of the optic nerve head.

Instrumentation

The principle of the imaging technique is shown in Figure 1. A diode laser beam at 532 nm was expanded, focused to a narrow line, and projected at an oblique angle on the retina after intravenous injection of the probe. A 2D phosphorescence optical section retinal image in the *Y-Z* retinal plane was acquired by placing a near-infrared filter, with transmission overlapping the phosphorescence emission of the oxygen probe, in front of the imaging camera. Because the incident laser beam was not coaxial with the viewing path, structures at various depths on the phosphorescence optical section image appeared laterally displaced according to their depth location. Instrumentation for image acquisition has been previously described.[39] The schematic diagram of the modified system for 3D phosphorescence imaging is shown in Figure 2. A galvanometer scanner (National Instruments, Woburn, MA) was incorporated in the system for scanning the laser beam horizontally on the retina. The laser line was scanned in small horizontal steps of 9 ± 3 μm across a retinal area of 198 to 423 μm in the horizontal direction and approximately 750 to 1010 μm in the vertical direction, contingent on the curvature of the eye and the dilation of the pupil. A series of 2D optical section phosphorescence images (range, 22–47) was generated from spatially adjacent locations. At each scan location, a set of phase-delayed phosphorescence optical section images was acquired by incrementally delaying the modulated intensifier of the imaging camera with respect to the modulated excitation laser beam, as previously described.[39]

Image Processing and Analysis

The 2D optical section phosphorescence images in the *Y-Z* retinal plane were processed to generate 3D phosphorescence retinal images at different retinal depths. Every third optical section phosphorescence image from a series of 34 images acquired during a laser scan is displayed in Figure 3 (top). Each 2D optical section phosphorescence image was segmented into eight vertical slices in depth by an automated software algorithm developed in Matlab (The Mathworks Inc., Natick, MA). The eight slices were separated in depth by 20 μm and encompassed the retinal thickness. The first slices from each 2D optical section phosphorescence images in the series were placed next to each other to construct an en face phosphorescence intensity image of the first retinal vascular layer. An example of the reconstructed en face phosphorescence intensity image of layer 5, generated by combining the fifth slice from each image, is shown in Figure 3 (middle). This process was repeated to generate a set of eight en face phosphorescence intensity images of retinal layers, separated by 20 μm in depth (Fig. 3, bottom). For each depth-displaced layer, a set of phase-delayed phosphorescence intensity images was constructed using the same reconstruction technique.

The methodology for quantitative measurement of PO_2 based on 2D phase-delayed phosphorescence intensity images has been previously described.[39] A frequency-domain approach was used for measurement of phosphorescence lifetime by varying the phase delay between the modulated excitation laser and the sensitivity of the phosphorescence imaging camera.[35,41] The PO_2 was determined from the lifetime according to the Stern-Volmer expression: $PO_2 = (\tau_0/\tau - 1)/(\kappa_Q)(\tau_0)$, where τ is the phosphorescence lifetime and κ_Q and τ_0 are the probe's quenching constant and lifetime in a zero oxygen environment, respectively. PO_2 was calculated at each pixel on the image with previously published κ_Q and τ_0 values of 381 mm $Hg^{-1} \cdot s^{-1}$ and 637 μs, respectively.[42] Three-dimensional PO_2 images were generated by mapping PO_2 in each of the eight depth-displaced retinal layers.

To determine PO_2 in the choroid, retinal arteries, and veins, PO_2 images were processed. A mask was generated by global thresholding of the phosphorescence intensity image (at zero

phase delay) for each layer. The mask assigned a value of 0 or 1 to image pixels based on intensity levels. The mask was multiplied by the PO_2 map for each corresponding layer. Regions of interest were selected on a layer closest to the choroid and a layer on which a retinal artery and vein were visible. Average PO_2 measurement in the choroid, retinal arteries, and veins was calculated. For determining PO_2 in the retinal capillaries, a mask was generated by local thresholding of the phosphorescence intensity image (at zero phase delay) for a layer on which capillaries were best visualized and in a region between a retinal artery and a vein. The mask was multiplied by the PO_2 map for the corresponding layer, and average PO_2 in the capillaries was calculated. To eliminate the contribution of noise caused by light scatter, only best-fitted phase-angle calculations ($R^2 > 0.9$) and PO_2 measurements within normal physiological conditions (<100 mm Hg) were included for calculation of averaged chorioretinal vascular PO_2 measurements.

Results

Examples of 3D phosphorescence intensity images and corresponding 3D PO_2 maps in an animal under room air breathing conditions (fraction inspired oxygen [FIO_2] = 21%) are shown in Figure 4. PO_2 measurements in the choroidal and retinal vasculatures are depicted by pseudocolors. The maps allowed visualization and quantitative measurement of PO_2 in the choroid and retinal vasculatures. Examples of a phosphorescence intensity image, a global, and a locally thresholded PO_2 map generated in one intraretinal layer are shown in Figure 5. Local thresholding allowed better visualization of retinal capillaries.

The blood pressure of the animals was relatively normal and remained unchanged during experiments. Blood pressure measurements were 110 ± 10 (mean ± SD) and 98 ± 24 mm Hg under normoxia (FIO_2 = 21%) and hypoxia (FIO_2 = 10%), respectively. A typical example of PO_2 maps generated in one animal in the study under normoxia and hypoxia are shown in Figure 6. Mean and SEM PO_2 were calculated in a layer closest to the choroid and in an intraretinal layer along a retinal artery and vein. Under normoxia, PO_2 in the choroid, retinal artery, and vein were 61.5 ± 0.3 (mean ± SEM), 60.4 ± 1.0, and 35.4 ± 0.9 mm Hg, respectively. Under hypoxia, PO_2 in the choroid, retinal artery, and vein were 41.2 ± 0.2, 28.2 ± 0.6, and 23.6 ± 1.0 mm Hg, respectively.

3D PO_2 Mapping under Normoxia

Mean and SEM of systemic arterial and chorioretinal vascular PO_2 measurements, derived based on 10 phase-delayed phosphorescence images, were calculated in nine rats under normoxia (FIO_2 = 21%; Fig. 7). Under normoxia, the systemic arterial and choroidal PO_2 were 65 ± 3 (mean ± SEM) and 58 ± 2 mm Hg, respectively. Choroidal PO_2 was significantly lower than systemic arterial PO_2 ($P = 0.02$). Retinal arterial, capillary, and venous PO_2 measurements were 47 ± 2 mm Hg, 44 ± 2 mm Hg, and 35 ± 2 mm Hg, respectively. Retinal vasculature PO_2 measurements were significantly lower than systemic arterial PO_2 ($P < 0.001$). Retinal venous PO_2 was significantly less than the PO_2 measured in the retinal artery, capillaries, and choroid ($P < 0.03$). The arteriovenous PO_2 difference was 12 ± 2 mm Hg under normoxia.

3D PO_2 Mapping under Hypoxia

Mean and SEM of systemic arterial and chorioretinal vascular PO_2 measurements were calculated in nine rats under hypoxia (FIO_2 = 10%; Fig. 7). Under hypoxia, chorioretinal vascular PO_2 measurements were decreased compared with values obtained under normoxia. There was no significant difference between systemic arterial PO_2 (40 ± 2 mm Hg) and choroidal PO_2 (41 ± 2 mm Hg; $P = 0.8$). Retinal arterial, capillary, and venous PO_2 measurements were 30 ± 2 mm Hg, 30 ± 2 mm Hg, and 23 ± 2 mm Hg, respectively. Retinal venous PO_2 was statistically lower than retinal arterial, capillary, and choroidal PO_2 ($P <$

0.004). The mean arteriovenous PO_2 difference was 7 ± 1 mm Hg, with a lower fraction of inspired oxygen.

Discussion

Assessment of retinal oxygenation is important for the diagnosis and understanding of many retinal diseases. In the present study, an optical section imaging system was reported, and its capability for 3D imaging of PO_2 in the chorioretinal vasculatures was demonstrated. Phosphorescence optical section images were acquired from closely spaced locations on the retina, segmented, and combined to construct en face images of vascular layers equally displaced in depth. Phase-delayed images were analyzed to generate PO_2 maps of the vasculature at different retinal depths. The validity of PO_2 maps was established by comparing measurements to systemic arterial PO_2 and demonstrating a decrease in retinal and choroidal PO_2 with decreased fractions of inspired oxygen.

Under normoxia (FIO_2 = 21%), systemic arterial PO_2 was lower than measurements obtained in previous studies.[43–45] As previously reported, the hypoxic condition of the rats in our study might have resulted from the respiratory depressant effect of the anesthetics because the rats were not intubated or ventilated and they breathed spontaneously.[46] Previous studies performed under systemic arterial PO_2 greater than 80 mm Hg in rat, monkey, miniature pig, and cat have reported choroidal PO_2 measurements that were approximately 60% of the systemic arterial PO_2.[4,43,47,48] In our previous study,[39] in which supplemental oxygen was provided to increase systemic arterial PO_2, we reported choroidal PO_2 values that were approximately 60% of systemic arterial PO_2, in agreement with published reports in cats and other species.[4,43,47,48] In the present study, choroidal PO_2 measurements averaged 58 mm Hg during normoxia (FIO_2 = 21%), comparable to other studies, despite the fact that the systemic arterial PO_2 was much lower (65 mm Hg here compared with more than 80 mm Hg in other studies).[4,43,47,48] This discrepancy may be attributed to the hypoxic condition of the rats in our study and the shape of the hemoglobin dissociation curve (hemoglobin saturation as a function of PO_2), which has the steepest slope at PO_2 values between approximately 20 and 60 mm Hg. Therefore, the same arteriovenous saturation difference (amount of oxygen extracted) will result in a smaller arteriovenous PO_2 difference at lower systemic arterial PO_2. Our findings are in accordance with findings of a previous study in cats,[4] which reported that choroidal PO_2 more closely approached systemic arterial PO_2 under hypoxia.

Retinal vascular PO_2 measurements were lower than data previously published in a study in rat using a similar phosphorescence imaging technique but with lower depth discrimination.[35] However, in the previous study, it was noted that measurements of PO_2 might have been artificially high because of contamination from the phosphorescence signal from the choroid. As expected, PO_2 measurements in retinal capillaries (44 mm Hg) were between measurements obtained in retinal arteries (47 mm Hg) and veins (35 mm Hg). Retinal capillary PO_2 was closer to retinal arterial PO_2, possibly because of the sampling location. In the present study, capillary PO_2 measurements were made within approximately 2 disc diameters of the optic nerve head. Given that retinal arterial and capillary PO_2 decreases with increasing distance from the optic nerve head because of oxygen diffusion along the length of the artery,[49] PO_2 in retinal capillaries close to the optic nerve head tends to be higher than PO_2 in retinal capillaries further away from the optic nerve head. To our knowledge, measurements of oxygen saturation in retinal capillaries have not been reported because of the small size of retinal capillaries, precluding reliable measurements. A notable advantage of our technique is that it allows measurements of PO_2 in retinal capillaries, thus providing a better means for assessing retinal tissue oxygenation than measuring PO_2 in large retinal blood vessels.

With a lower fraction of inspired oxygen, chorioretinal vascular PO_2 decreased compared with measurements under air breathing. A 39% decrease in systemic arterial PO_2 corresponded with a 30% decrease in choroidal PO_2, comparable to a 37% change in choroidal PO_2 measured in cats using a microelectrode technique.[4] Furthermore, a decrease in the mean arteriovenous PO_2 difference was observed with a lower fraction of inspired oxygen. During hypoxia, the PO_2 gradient from blood vessels to tissue decreases, and retinal vasculatures are known to dilate.[50,51] Dilation of the retinal vasculature would result in a decrease in oxygen extraction/volume and, hence, a decrease in arteriovenous PO_2 difference. Ideally, tissue oxygen consumption would not be affected, but it could be reduced if the increase in blood flow were insufficient.

Retinal arterial PO_2 decreased under hypoxic conditions, similar to retinal arterial oxygen-saturation changes reported in human subjects under acute hypoxic exposure.[52] Additionally, we demonstrated a reduction in retinal capillary PO_2 under hypoxia. Ideally, functional evaluation of the retina requires direct measurement of tissue PO_2 rather than of retinal vascular PO_2. However, mapping of retinal capillary PO_2 provides a better estimation of tissue PO_2 than measurements of oxygen saturation or tension in large retinal blood vessels. Overall, the retinal vascular PO_2 mapping capability of our technique is useful for identifying retinal regions made hypoxic from vascular diseases such as diabetic retinopathy and for studying oxygen gradients along retinal vasculatures. Detection of abnormalities in oxygen gradients may also be indicative of alterations in retinal tissue oxygen consumption caused by disease. The technique can provide knowledge of the relationship between retinal hypoxia, capillary nonperfusion, and development of retinal abnormalities. Furthermore, it makes possible a quantitative means for evaluating available and new experimental therapeutic regimens that aim to alleviate retinal hypoxia.

In summary, an optical imaging system for quantitative mapping of vascular PO_2 at different retinal depths was developed. Three-dimensional PO_2 maps demonstrated the potential of this technique for visualization and measurement of PO_2 in retinal microvasculatures needed to investigate the occurrence of early retinal oxygenation changes caused by disease. Even though the imaging system for mapping chorioretinal vascular PO_2 is limited to animal studies, the technique provides knowledge that can lead to better understanding of oxygen dynamics in health and disease. Findings from animal models of retinal diseases are valuable for assessing current therapeutic interventions and developing new treatment regimens for diseases in which retinal ischemia plays a role.

Acknowledgments

Supported by National Institutes of Health Grants EY17918 and EY01792, Pearle Vision Foundation, and Research to Prevent Blindness.

References

1. Linsenmeier RA. Effects of light and darkness on oxygen distribution and consumption in the cat retina. J Gen Physiol 1986;88:521–542. [PubMed: 3783124]
2. Linsenmeier RA, Yancey CM. Effects of hyperoxia on the oxygen distribution in the intact cat retina. Invest Ophthalmol Vis Sci 1989;30:612–618. [PubMed: 2703302]
3. Alder VA, Cringle SJ. Vitreal and retinal oxygenation. Graefes Arch Clin Exp Ophthalmol 1990;228:151–157. [PubMed: 2338253]
4. Linsenmeier RA, Braun RD. Oxygen distribution and consumption in the cat retina during normoxia and hypoxemia. J Gen Physiol 1992;99:177–197. [PubMed: 1613482]
5. Linsenmeier RA, Braun RD, McRipley MA, et al. Retinal hypoxia in long-term diabetic cats. Invest Ophthalmol Vis Sci 1998;39:1647–1657. [PubMed: 9699554]

6. Cringle SJ, Yu DY, Yu PK, Su EN. Intraretinal oxygen consumption in the rat in vivo. Invest Ophthalmol Vis Sci 2002;43:1922–1927. [PubMed: 12037000]
7. Wangsa-Wirawan ND, Linsenmeier RA. Retinal oxygen: fundamental and clinical aspects. Arch Ophthalmol 2003;121:547–557. [PubMed: 12695252]
8. Yu DY, Cringle SJ. Oxygen distribution in the mouse retina. Invest Ophthalmol Vis Sci 2006;47:1109–1112. [PubMed: 16505048]
9. Padnick-Silver L, Kang Derwent JJ, Giuliano E, Narfstrom K, Linsenmeier RA. Retinal oxygenation and oxygen metabolism in Abyssinian cats with a hereditary retinal degeneration. Invest Ophthalmol Vis Sci 2006;47:3683–3689. [PubMed: 16877443]
10. Cringle SJ, Yu PK, Su EN, Yu DY. Oxygen distribution and consumption in the developing rat retina. Invest Ophthalmol Vis Sci 2006;47:4072–4076. [PubMed: 16936126]
11. Yu DY, Cringle SJ, Yu PK, Su EN. Intraretinal oxygen distribution and consumption during retinal artery occlusion and graded hyperoxic ventilation in the rat. Invest Ophthalmol Vis Sci 2007;48:2290–2296. [PubMed: 17460293]
12. Chung CK, Linsenmeier RA. Effect of carbogen (95% O_2/5% CO_2) on retinal oxygenation in dark-adapted anesthetized cats. Curr Eye Res 2007;32:699–707. [PubMed: 17852195]
13. Berkowitz BA, Kowluru RA, Frank RN, Kern TS, Hohman TC, Prakash M. Subnormal retinal oxygenation response precedes diabetic-like retinopathy. Invest Ophthalmol Vis Sci 1999;40:2100–2105. [PubMed: 10440266]
14. Berkowitz BA, Luan H, Gupta RR, et al. Regulation of the early subnormal retinal oxygenation response in experimental diabetes by inducible nitric oxide synthase. Diabetes 2004;53:173–178. [PubMed: 14693712]
15. Ito Y, Berkowitz BA. MR studies of retinal oxygenation. Vision Res 2001;41:1307–1311. [PubMed: 11322975]
16. Riva CE. Noninvasive measurement of oxygen tension in the optic nerve head. Curr Opin Ophthalmol 1998;9:56–60. [PubMed: 10180515]
17. Zhang W, Ito Y, Berlin E, Roberts R, Berkowitz BA. Role of hypoxia during normal retinal vessel development and in experimental retinopathy of prematurity. Invest Ophthalmol Vis Sci 2003;44:3119–3123. [PubMed: 12824260]
18. Roberts R, Zhang W, Ito Y, Berkowitz BA. Spatial pattern and temporal evolution of retinal oxygenation response in oxygen-induced retinopathy. Invest Ophthalmol Vis Sci 2003;44:5315–5320. [PubMed: 14638732]
19. Delori FC. Noninvasive technique for oximetry of blood in retinal vessels. Appl Opt 1988;27:1113–1125. [PubMed: 20531526]
20. Smith MH, Denninghoff KR, Hillman LW, Chipman RA. Oxygen saturation measurements of blood in retinal vessels during blood loss. J Biomed Opt 1998;3:296–303.
21. Schweitzer D, Thamm E, Hammer M, Kraft J. A new method for the measurement of oxygen saturation at the human ocular fundus. Int Ophthalmol 2001;23:347–353. [PubMed: 11944861]
22. Hammer M, Schweitzer D. Quantitative reflection spectroscopy at the human ocular fundus. Phys Med Biol 2002;47:179–191. [PubMed: 11837611]
23. Denninghoff KR, Smith MH, Lompado A, Hillman LW. Retinal venous oxygen saturation and cardiac output during controlled hemorrhage and resuscitation. J Appl Physiol 2003;94:891–896. [PubMed: 12571124]
24. Crittin M, Schmidt H, Riva CE. Hemoglobin oxygen saturation (SO_2) in the human ocular fundus measured by reflectance oximetry: preliminary data in retinal veins. Klin Monatsbl Augenheilkd 2002;219:289–291. [PubMed: 12022020]
25. Ito M, Murayama K, Deguchi T, et al. Oxygen saturation levels in the juxta-papillary retina in eyes with glaucoma. Exp Eye Res 2008;86:512–518. [PubMed: 18262523]
26. Beach J, Ning J, Khoobehi B. Oxygen saturation in optic nerve head structures by hyperspectral image analysis. Curr Eye Res 2007;32:161–170. [PubMed: 17364749]
27. Arimoto H, Furukawa H. Retinal blood oxygen saturation mapping by multispectral imaging and morphological angiography. Conf Proc IEEE Eng Med Biol Soc 2007;2007:1627–1630. [PubMed: 18002284]

28. Zuckerman R, Cheasty JE, Wang Y. Optical mapping of inner retinal tissue PO2. Curr Eye Res 1993;12:809–825. [PubMed: 8261793]
29. Wilson DF, Vanderkooi JM, Green TJ, Maniara G, DeFeo SP, Bloom-garden DC. A versatile and sensitive method for measuring oxygen. Adv Exp Med Biol 1987;215:71–77. [PubMed: 3673745]
30. Rumsey WL, Vanderkooi JM, Wilson DF. Imaging of phosphorescence: a novel method for measuring oxygen distribution in perfused tissue. Science 1988;241:1649–1651. [PubMed: 3420417]
31. Shonat RD, Wilson DF, Riva CE, Pawlowski M. Oxygen distribution in the retinal and choroidal vessels of the cat as measured by a new phosphorescence imaging method. Appl Optics 1992;31:3711–3718.
32. Shonat RD, Wilson DF, Riva CE, Cranstoun SD. Effect of acute increases in intraocular pressure on intravascular optic nerve head oxygen tension in cats. Invest Ophthalmol Vis Sci 1992;33:3174–3180. [PubMed: 1399424]
33. Buerk DG, Shonat RD, Riva CE, Cranstoun SD. O_2 gradients and countercurrent exchange in the cat vitreous humor near retinal arterioles and venules. Microvasc Res 1993;45:134–148. [PubMed: 8361397]
34. Shonat RD, Johnson PC. Oxygen tension gradients and heterogeneity in venous microcirculation: a phosphorescence quenching study. Am J Physiol 1997;272:H2233–H2240. [PubMed: 9176291]
35. Shonat RD, Kight AC. Oxygen tension imaging in the mouse retina. Ann Biomed Eng 2003;31:1084–1096. [PubMed: 14582611]
36. Ferrez PW, Chamot SR, Petrig BL, Pournaras CJ, Riva CR. Effect of visual stimulation on blood oxygenation in the optic nerve head of miniature pigs: a pilot study. Klin Monatsbl Augenheilkd 2004;221:364–366. [PubMed: 15162281]
37. Shahidi M, Blair NP, Mori M, Zelkha R. Feasibility of noninvasive imaging of chorioretinal oxygenation. Ophthalmic Surg Lasers Imaging 2004;35:415–422. [PubMed: 15497552]
38. Shakoor A, Shahidi M, Blair NP, Mori M. Noninvasive assessment of chorioretinal oxygenation changes in experimental carotid occlusion. Curr Eye Res 2005;30:763–771. [PubMed: 16146922]
39. Shahidi M, Shakoor A, Shonat R, Mori M, Blair NP. A method for measurement of chorioretinal oxygen tension. Curr Eye Res 2006;31:357–366. [PubMed: 16603469]
40. ANSI. American National Standard for Safe Use of Lasers—ANSI Z136.1–1993. Orlando, FL: The Laser Institute of America; 1993.
41. Lakowicz JR, Szmacinski H, Nowaczyk K, Berndt KW, Johnson M. Fluorescence lifetime imaging. Anal Biochem 1992;202:316–330. [PubMed: 1519759]
42. Lo LW, Koch CJ, Wilson DF. Calibration of oxygen-dependent quenching of the phosphorescence of Pd-meso-tetra (4-carboxyphenyl) porphine: a phosphor with general application for measuring oxygen concentration in biological systems. Anal Biochem 1996;236:153–160. [PubMed: 8619481]
43. Yu DY, Cringle SJ. Oxygen distribution and consumption within the retina in vascularised and avascular retinas and in animal models of retinal disease. Prog Retin Eye Res 2001;20:175–208. [PubMed: 11173251]
44. Torbati D, Totapally BR, Camacho MT, Wolfsdorf J. Experimental critical care in ventilated rats: effect of hypercapnia on arterial oxygen-carrying capacity. J Crit Care 1999;14:191–7. [PubMed: 10622754]
45. Sumitra M, Manikandan P, Rao KV, Nayeem M, Manohar BM, Puvanakrishnan R. Cardiorespiratory effects of diazepam-ketamine, xylazine-ketamine and thiopentone anesthesia in male Wistar rats—a comparative analysis. Life Sci 2004;75:1887–1896. [PubMed: 15302232]
46. Shakoor A, Gupta M, Blair NP, Mori M, Shahidi M. Chorioretinal vascular oxygen tension in spontaneously breathing anesthetized rats. Ophthalmic Res 2007;39:103–107. [PubMed: 17284937]
47. Yu DY, Cringle SJ, Su EN. Intraretinal oxygen distribution in the monkey retina and the response to systemic hyperoxia. Invest Ophthalmol Vis Sci 2005;46:4728–4733. [PubMed: 16303972]
48. Pournaras CJ, Riva CE, Tsacopoulos M, Strommer K. Diffusion of O_2 in the retina of anesthetized miniature pigs in normoxia and hyperoxia. 1989;49:347–360.
49. Shakoor A, Blair NP, Mori M, Shahidi M. Chorioretinal vascular oxygen tension changes in response to light flicker. Invest Ophthalmol Vis Sci 2006;47:4962–4965. [PubMed: 17065514]

50. Pournaras C, Tsacopoulos M, Chapuis P. Studies on the role of prostaglandins in the regulation of retinal blood flow. Exp Eye Res 1978;26:687–697. [PubMed: 680025]

51. Pournaras CJ, Rungger-Brändle E, Riva CE, Hardarson SH, Stefansson E. Regulation of retinal blood flow in health and disease. Prog Retin Eye Res 2008;27:284–330. [PubMed: 18448380]

52. Janaky M, Grosz A, Toth E, Benedek K, Benedek G. Hypobaric hypoxia reduces the amplitude of oscillatory potentials in the human ERG. Doc Ophthalmol 2007;114:45–51. [PubMed: 17211646]

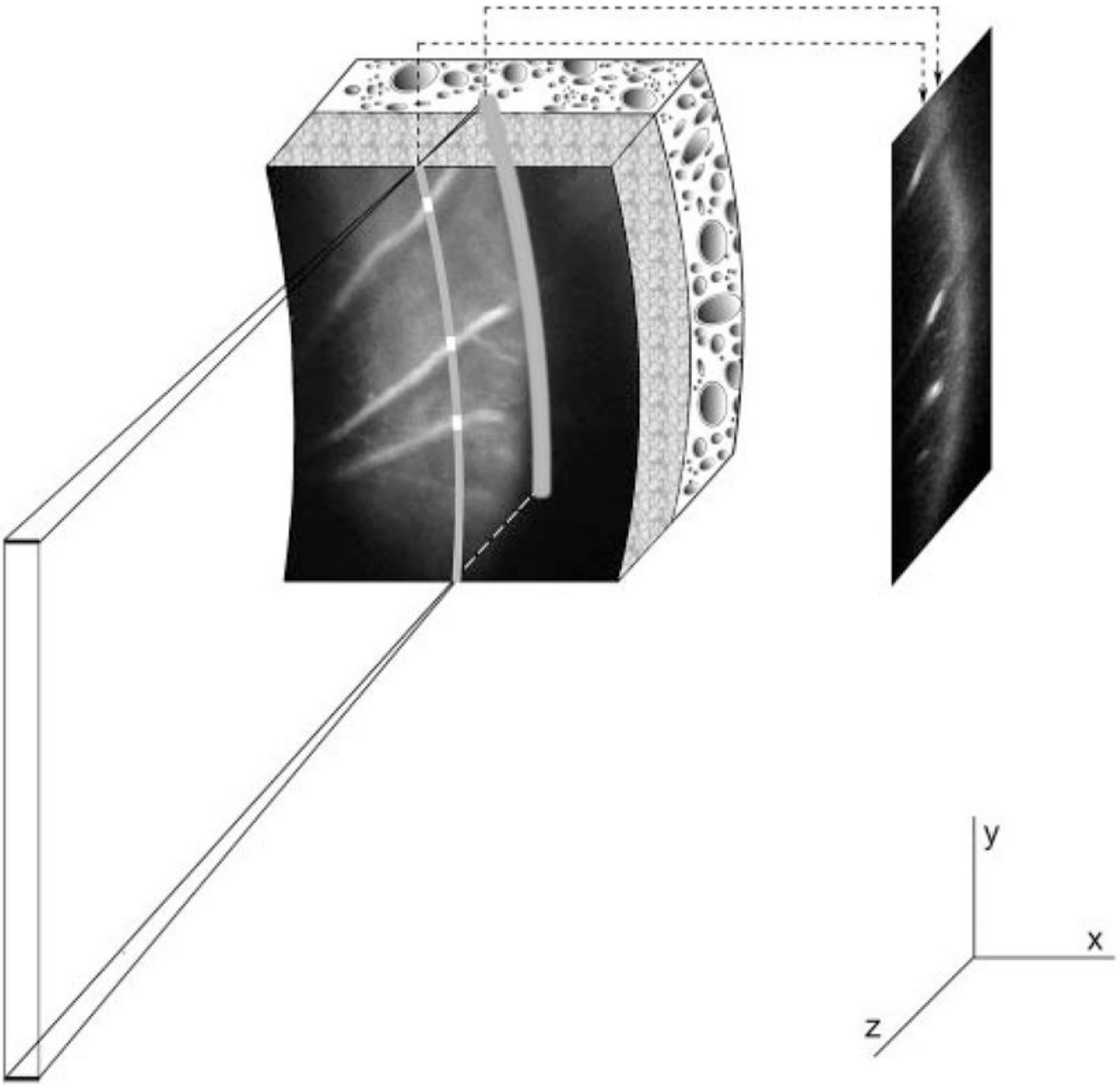

Figure 1.

A laser beam was projected at an oblique angle onto the retina after intravenous injection of an oxygen-sensitive molecular probe to generate an optical section phosphorescence image in the *Y-Z* plane of the retina. Since the incident laser beam was not coaxial with the viewing axis, chorioretinal vasculatures appeared laterally displaced according to their depth location on the phosphorescence optical section image.

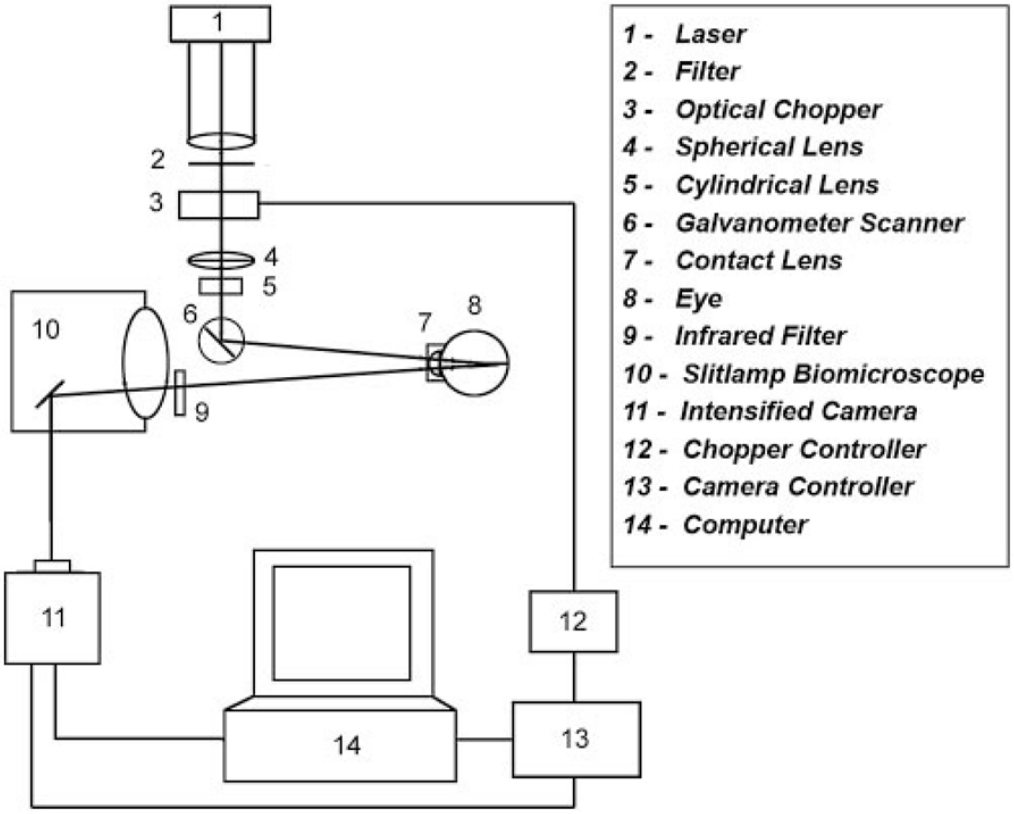

Figure 2.
Diagram of the instrument for 3D chorioretinal oxygen-tension mapping.

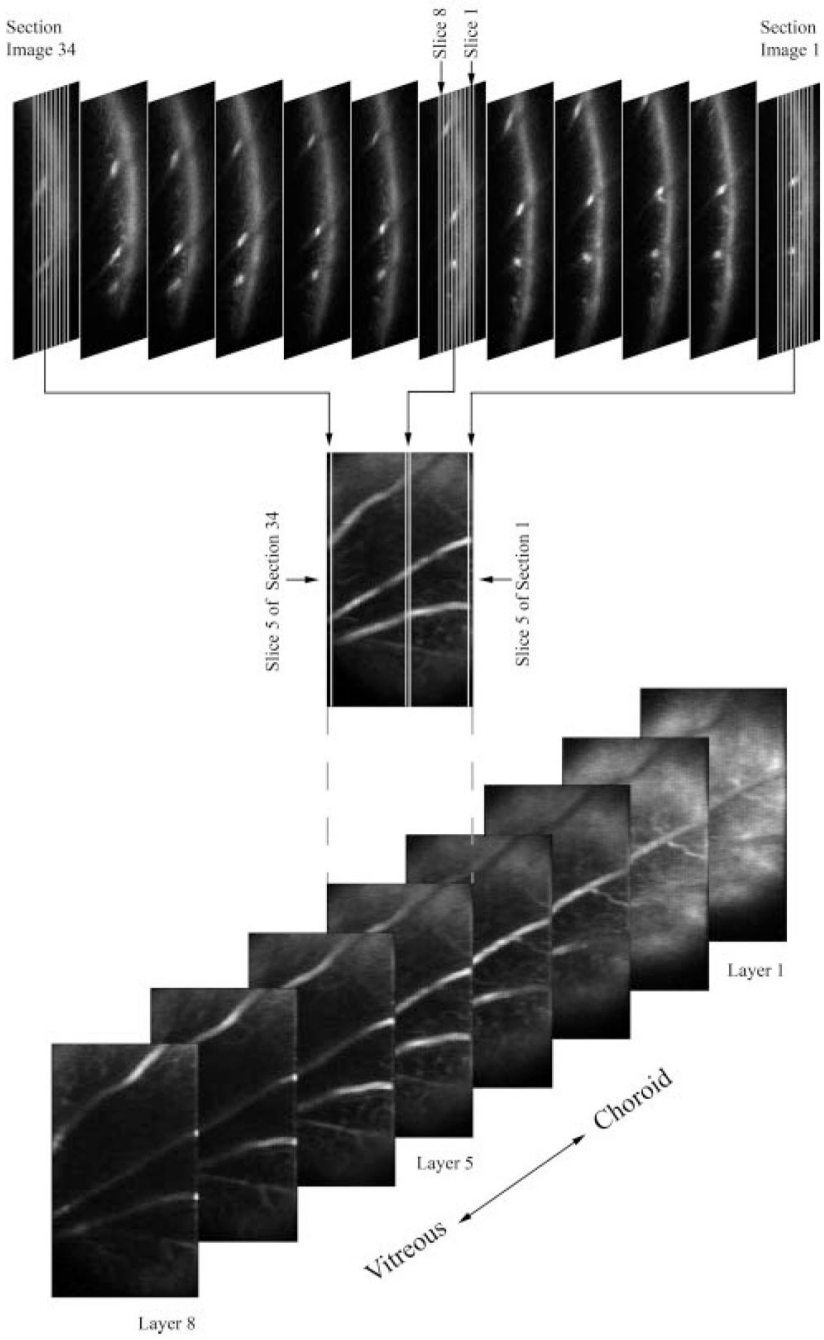

Figure 3.

Top: every third optical section phosphorescence image from a series of 34 images acquired during a laser scan is displayed. *Middle*: an en face phosphorescence intensity image of layer 5 was reconstructed by automatically segmenting every optical section phosphorescence image into eight slices and combining the fifth slice from each image. *Bottom*: reconstructed en face phosphorescence intensity images of eight retinal layers, displaced equally in depth.

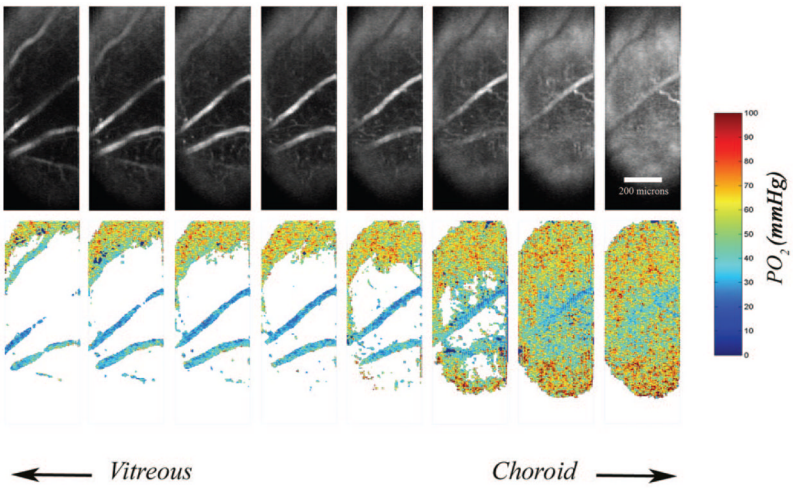

Figure 4.

Phase-delayed phosphorescence intensity images were analyzed by customized computer software to generate three-dimensional oxygen-tension maps. *Top*: three-dimensional phosphorescence intensity images at zero phase delay. *Bottom*: three-dimensional oxygen-tension maps allowed visualization and quantitative measurement of oxygen tension in the chorioretinal vasculatures. On the top portion of the oxygen-tension maps, in layers closer to the vitreous, a sampling of choroidal oxygen tension can be observed because of the curvature of the globe.

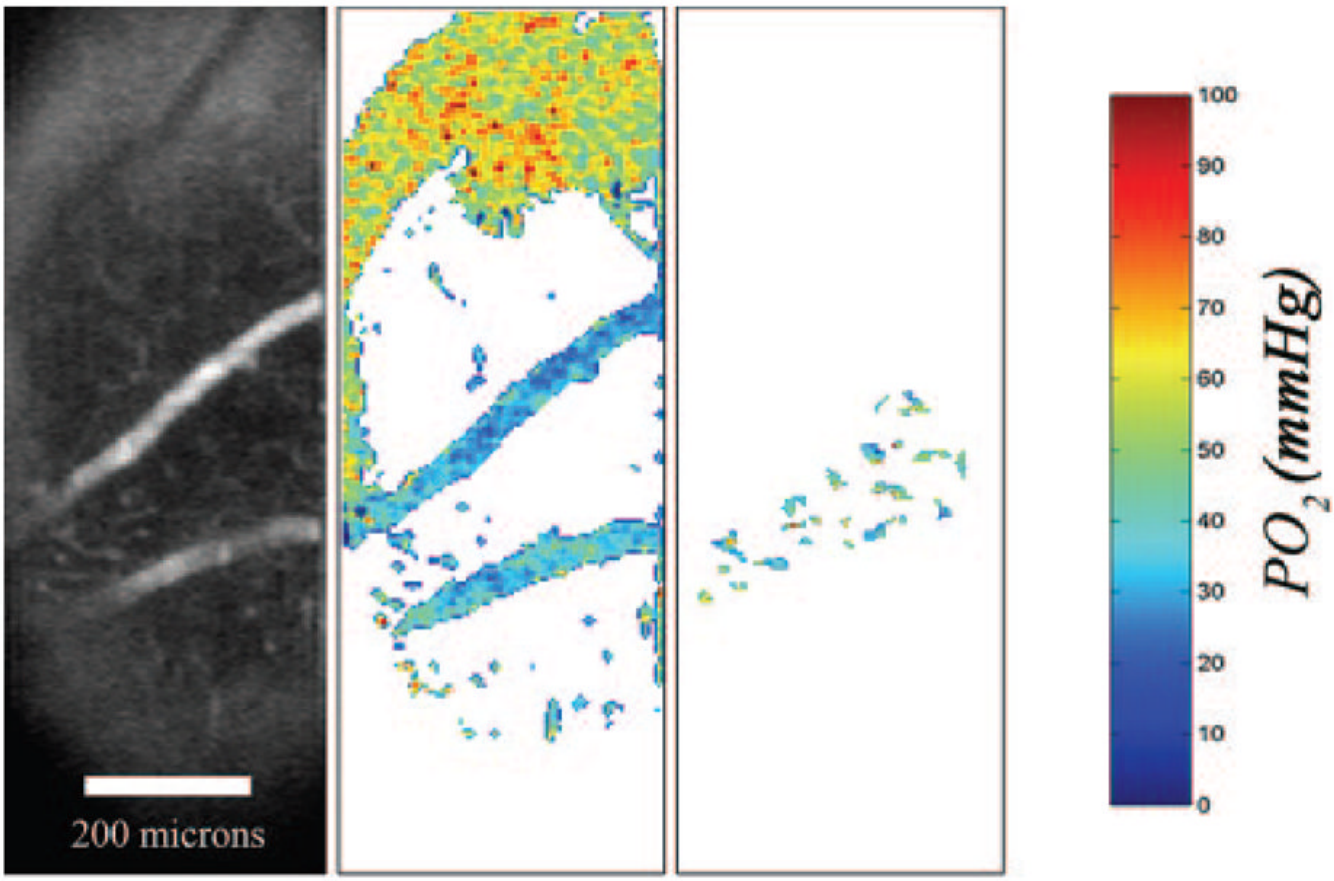

Figure 5.
Left: example of a phosphorescence intensity image from a retinal layer. *Middle*: corresponding oxygen-tension map after global thresholding for visualizing the retinal artery and vein. *Right*: corresponding oxygen-tension map after local thresholding for visualization of retinal capillaries.

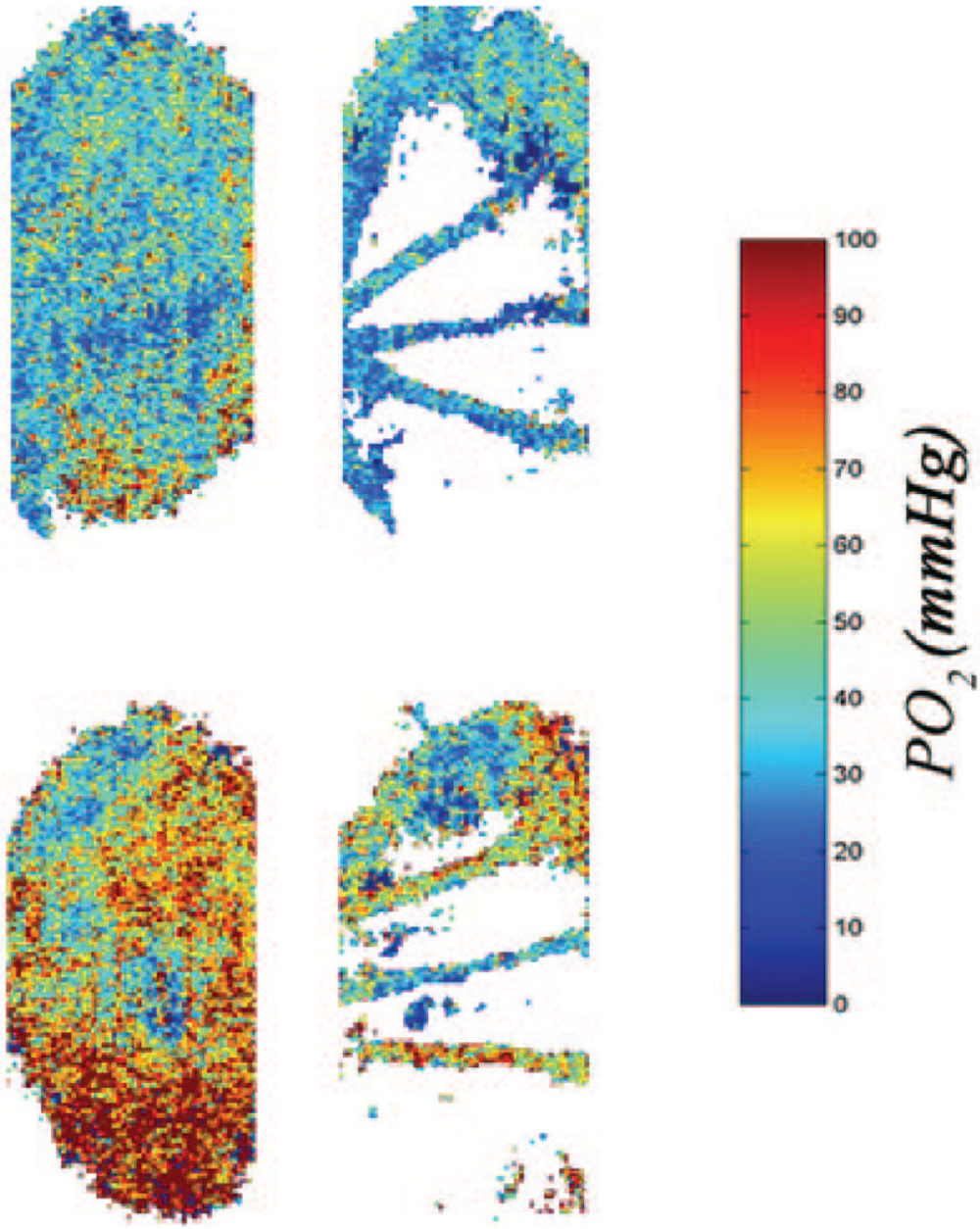

Figure 6.
Typical oxygen-tension maps generated in a rat under hypoxia (*top*) and normoxia (*bottom*). Oxygen-tension changes in the choroid (*left*) and retinal artery and vein (*right*) can be visualized.

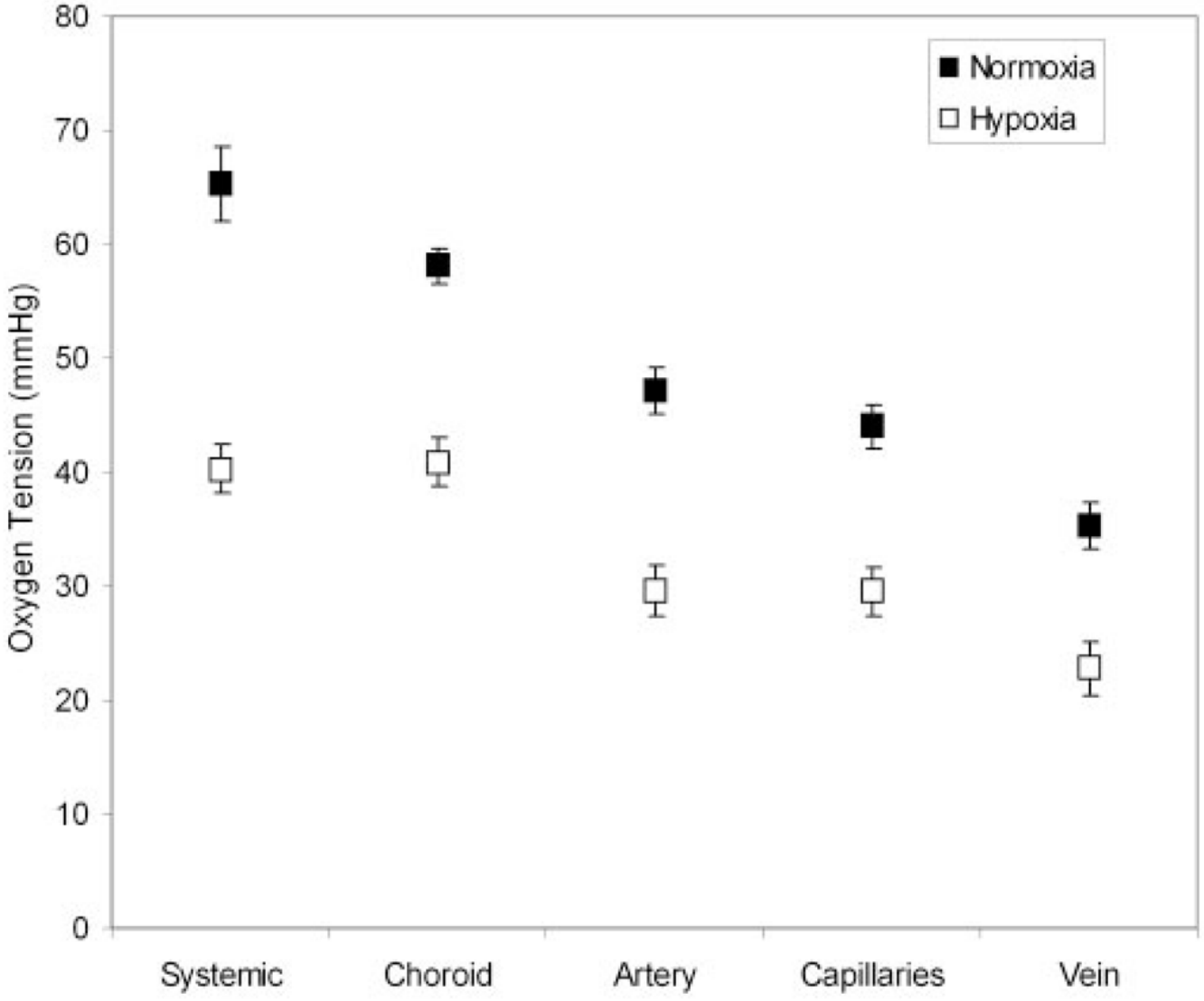

Figure 7.
Mean oxygen-tension measurements in the systemic artery, choroid, and retinal vasculatures under normoxia (air-breathing condition) and hypoxia (10% oxygen-breathing condition), compiled from data in nine rats. Error bars represent SEM.